*applied sciences*

MDPI

*Article*

# Investigating the Effect of Lubricating Oil Volatility and Ash Content on the Emission of Sub-23 nm Particles

**Salvatore Lagana, Sebastian A. Pfau, Ephraim Haffner-Staton, Antonino La Rocca * and Alasdair Cairns**

Department of Mechanical Materials and Manufacturing Engineering, University of Nottingham, Nottingham NG7 2RD, UK; ezxsl9@exmail.nottingham.ac.uk (S.L.); alasdair.cairns1@nottingham.ac.uk (A.C.)
* Correspondence: antonino.larocca@nottingham.ac.uk

**Featured Application: This work highlights the critical role of oil formulation in minimizing sub-23 nm particulates; it is particularly relevant in emerging $H_2$ and $NH_3$ engines, crucial for meeting stricter SPN emission standards in decarbonized fuel platforms.**

**Abstract:** As the world transitions to decarbonized fuels, understanding the impact of engine oil on emissions remains crucial. Lubricant-derived particulate emissions can influence air quality and regulatory compliance in future transport. Researchers have predominantly focused on transient driving cycles to replicate real-world conditions and capture the full range of particle size. This emphasis has led to a lack of comprehensive data on oil-related particulate emissions during steady-state operations, particularly for particles smaller than 23 nm. This paper addresses this gap as upcoming regulations, such as Euro 7, are expected to impose stricter limits by extending measurement thresholds down to 10 nm. The investigation was conducted on a 1.0 L gasoline direct injection engine, assessing total particulate number (TPN) emissions using three oil formulations: a baseline oil with mid-ash content and mid-volatility, a low-ash and low-volatility oil (LoLo), and a high-ash and high-volatility oil (HiHi). A DMS500, with and without a catalytic stripper, measured particle size distribution and TPN. Two digital filters were applied to obtain particle number (PN) metrics comparable to condensation particle counters: "F1-PN > 23" with d50 = 23 nm and "F3-PN > 10" with d50 = 10 nm. Sub-23 nm particles dominated emissions, with baseline oil generally producing higher PN emissions except at low loads. Using F1-PN > 23, HiHi exhibited higher PN counts across moderate to high speeds, while F3-PN > 10 revealed lower PN emissions for HiHi at specific conditions, excluding 2250 rpm-fast idle. By a weighted arithmetic mean, HiHi's emissions were 9.7% higher than LoLo with F1-PN > 23 and 3.6% higher with F3-PN > 10. Oil formulation did not influence nucleation mode diameter. A three-way ANOVA demonstrated that load and speed were the predominant factors affecting emissions over the entire testing map; albeit at specific operating conditions the effect of the oil is evident. This suggests that under steady-state conditions, carbon-based fuel still plays a key role in particle formation. Future work will investigate decarbonised fuels to further isolate the effect of oil on emissions.

**Keywords:** gasoline direct injection (GDI); oil formulation; sub-23 nm; particle number (PN); catalytic stripper; DMS500; soot; particulate emission



Academic Editors: Rafał Rajczyk and Rafał Kobyłecki

Received: 18 January 2025
Revised: 10 February 2025
Accepted: 17 February 2025
Published: 19 February 2025

**Citation:** Lagana, S.; Pfau, S.A.; Haffner-Staton, E.; La Rocca, A.; Cairns, A. Investigating the Effect of Lubricating Oil Volatility and Ash Content on the Emission of Sub-23 nm Particles. *Appl. Sci.* **2025**, *15*, 2212. https://doi.org/10.3390/app15042212



## 1. Introduction

Soot is one of the main risk factors causing millions of deaths, ranked 6th highest by the global burden of disease (GBD) analysis in 2018 from 2016 data [1]. On the same

note, the World Health Organisation (WHO) in a report from 2016 [2] approximated the number of deaths that can be linked to particulate pollution close to 4.2 million yearly, with more than 90% of people exposed to dangerous quantities of PM2.5 (particulate matter <2.5 microns) worldwide. This is because soot is a well-known cause of diseases of the lungs and heart [3,4] with the smallest, PM0.1, being the most harmful, as they can penetrate deeper and result in various conditions in multiple organs [3,5–7]. In environmental terms, black carbon (which also includes soot) is one of the main global warming agents, third compared to $CO_2$ and $CH_4$ [8,9]. This is due to its light absorption characteristic; it can heat its surroundings with a warming impact of about 450–1500 times higher than $CO_2$ per unit mass [10]. However, due to its short life in the atmosphere, black carbon emissions reduction can have more rapid benefits, slowing down climate change at a more significant rate [9,10]. From simulation work, it was shown that eliminating fossil fuel organic matter and black carbon in the atmosphere can bring net warming down by 20–45% within only 3–5 years, while the same effect with $CO_2$ would be achieved by reducing it by a third and would take about 50–200 years [9,11]. Transport alone is responsible for 26% of black carbon [10] emissions as soot is emitted from internal combustion engine vehicles (ICEVs) as a combustion by-product. Although the shift to electric vehicles is now imminent with ICEV sales banned or restricted by countries from 2025 onwards [12], these will continue to exist on the road without limitation in the used market. Another at least 25 years are expected with ICEVs around [13]. For this reason, together with soot's short atmospheric life, research to reduce soot emissions and understand the particles being emitted is greatly significant to progress in the climate change fight.

Soot is generated in the incomplete combustion of hydrocarbons [14], where the fuel is in excess, locally in the chamber. The main events where this occurs are diffusion combustion droplets close to the injector, improper mixing during stratified combustion, and pool fire (owing to spray depositing on piston/cylinder walls) [15,16]. Generally, the high complexity of hydrocarbon chemistry during combustion has made comprehension of how these particles form extremely difficult [17,18]. Overall, the current understanding of soot formation can be divided into five phases: nucleation, mass growth, coagulation, carbonisation, and oxidation [18–20]. Nucleation is where PAHs (polycyclic hydrocarbons) form, which are seen as soot's first molecular precursors [18–21]. Mass growth involves further PAHs condensation and additional carbon inclusion through the hydrogen abstraction–acetylene addition (HACA) mechanism [18–20], which allows for size increase. Nucleation-mass growth gives rise to the smallest single building blocks of soot known as primary particles constituted of a core, shell, and amorphous layer [15]. Coagulation consists of bundles and clusters being formed by primary particles sticking together, originating agglomerations [18–20,22]. These are also known as secondary particles and can have chain-like or clustered structures [14]. Carbonisation, not always found, describes amorphic to graphitic carbon conversion in soot in some local regions [19,23]. Finally, oxidation burns away the particles by reacting with oxygen at high temperatures [20,23]. During combustion, all these stages are fast and can take place simultaneously, but this seems to be the overall particles' formation order.

Soot emissions have been studied extensively from diesel engines [21,24] as they are 10× higher than port fuel injection engines [25]. These have always been maintained under control through the use of diesel particulate filters. However, in the last decade, due to the advent of gasoline direct injection (GDI) technology to diminish $CO_2$ emissions, also propelled by concerns regarding excessive $NO_x$ emissions of diesel engines [26], GDI soot has also been observed. This is quantitatively similar to diesel, and therefore, the study of its soot becomes fundamental to understanding whether it can be tackled equivalently by

using new gasoline particulate filters (GPFs), which are the same concept as the diesel ones but with different design requirements.

Current regulation, Euro 6, restricts only >23 nm particles not to be more than $6 \times 10^{11}$/km [27,28]. This threshold is due to knowledge from past diesel studies and, above all, due to past measurement limitations, which could measure with a maximum detection efficiency of 50% at 23 nm and 90% at 41 nm (d50 = 23 nm and d90 = 41 nm) [29]. This limit is defined by the particle measurement protocol (PMP) and is known as SPN23 (solid particle number), based on the accuracy of particle number counters (PNCs) as reference measuring devices. Over the last years, as more evidence is showing more presence of SPN below 23 nm also for past technologies [28,30,31], new regulations are expected to get tighter with Euro 7. The Consortium for Ultra-low Vehicle Emissions (CLOVE), which is made up of emissions experts across Europe, has proposed for Euro 7 a limit of $1 \times 10^{11}$/km for particles >10 nm [13]. In Table 1, CLOVE propositions for Euro 7 are summarised. Eventually, the European Commission on 10 November 2022 proposed the limits [32] highlighted in the last row of the table, which may become effective from 2025.

**Table 1.** Euro 7 CLOVE proposition (adapted from [13]).

| Regulation | Nitrogen Oxides (NOx) | Particulate Number (PN) | Particulate Mass (PM) | Carbon Monoxide (CO) | Non-Methane Organic Gases (NMOGs) |
|---|---|---|---|---|---|
| Euro 6 (Current) | 80 mg/km | $6 \times 10^{11}$/km including all >23 nm particles (SPN23) | 4.5 mg/km | 1000 mg/km | 68 mg/km |
| Euro 7 (CLOVE) | 20 mg/km | $1 \times 10^{11}$/km including all >10 nm particles (SPN10) | 2 mg/km | 400 mg/km | 25 mg/km |
| Euro 7 (European Commission) | 60 mg/km | $6 \times 10^{11}$/km including all >10 nm particles (SPN10) | 4.5 mg/km | 500 mg/km | 68 mg/km |

Samaras et al. [33] carried out a study comparing SPN10 to SPN23 emissions, which showed that with a $6 \times 10^{11}$/km limit, SPN10 would still accept most of the vehicles but with $1 \times 10^{11}$/km might become too stringent, affecting a large quantity of existing vehicles.

The reason for choosing 10 nm as the new standard is owing to the improvements in measurement capabilities achieved by the European Union's Horizon 2020 research and innovation program. This funded three projects to explore the possibility of passing from an SPN23 to an SPN10 standard, with d50 = 10 nm and d90 = 23 nm [34]. These projects are DownToTen, PEMs4Nano, and SUREAL-23 [34]. The former two focused on developing a new PEMS (portable emissions measurement system) to quantify particle numbers (PNs) of current and future vehicle technologies for both laboratory and RDE (real driving emissions). On the other hand, the latter concentrated its efforts on producing new technologies to solve exhaust sampling and treatment methodology issues [34]. All of these contributed to attaining d50 = 10 nm for the new SPN10 regulation.

An alternative method to find TPN or SPN is by using a DMS (differential mobility spectrometer). One of the most common commercially available DMS machines used in research is Cambustion DMS500. Generally, this is mainly utilised to find PSD (particle size distribution), but with the use of empirical approximations based on instrument calibrations, the particle count from DMS500 can be obtained [35]. One method to convert PSD to PMP-comparable was with lognormal fitting [35,36]. This was effective for the SPN23 standard with d50 = 23 nm and d90 = 41 nm. However, for the implementation of the newly discussed SPN10, where sub-23 nm particles are observed, lognormal fitting is no longer viable due to fitting modes being close to prescribed size limits, substantially decreasing its reliability [35,36].

Another way to obtain the PMP equivalent TPN from the DMS is to use digital filtering (DF) [35–37]. The equation below (where dp is the particle diameter) was proposed by Leach [35] and employed in some studies [38,39], showing results representative of the

SPN23 standard. As DMS has a higher particle size resolution than the condensation particle counter (CPC), capturing particles down to 5 nm, digital filtering works by prescribing the SPN23 detection efficiencies with the filter [35] and suppressing the high-level noise for sub-23 nm particles. A Wiebe function structure was adopted for the filtering operation [35,36].

$$f(d_p) = \begin{Bmatrix} 1 - exp\left[-3.54\left(\frac{d_p - 14}{40}\right)^{1.09}\right], & d \geq 14 \\ 0, & d < 14 \end{Bmatrix} \quad (1)$$

This was validated in [35], where results from DMS500 Wiebe were compared to AVL CPC (called APC) with SPN23 detection efficiencies. Therefore, this equation can be applied to prescribe CPC detection efficiency of d50 = 23 nm and d90 = 41 nm on DMS500 PSD data.

Two more digital filters were proposed by Leach et al. [40] and one by Pfau et al. [36] to model counting efficiencies that have been proposed for future SPN10 regulations. However, these would need to be validated against a CPC with the same detection efficiency as it was done for Equation (1). Pfau et al.'s [36] equation to prescribe detection efficiency of d65 = 10 nm and d90 = 15 nm is reported here in Equation (2).

$$f(d_p) = \begin{Bmatrix} 1 - exp\left[-5\left(\frac{d_p - 5}{20}\right)^{1.12}\right], & d \geq 5 \\ 0, & d < 5 \end{Bmatrix} \quad (2)$$

In the following, the two digital filters used in this study are referred to as "F1-PN > 23" for d50 = 23 nm and d90 = 41 nm and "F3-PN > 10" for d65 = 10 nm and d90 = 15 nm. This naming is in line with the study by Pfau et al. in [37] that used these same two filters. Many studies have been performed to understand the relationship between soot and engine running conditions, engine metrics (air-to-fuel ratio—AFR, spark timing, start of injection—SOI, mass of fuel burnt—MFB, exhaust temperature), or fuel type. Pfau et al. [41], using a DMS with and without a catalytic stripper (CS), found that the engine emits most particles at fast idling conditions at 0 Nm-1250 rpm, while the lowest amount was at 20 Nm-2250 rpm. In this experiment, it was noticed that a high level of total unburned hydrocarbons (THCs) encourages higher solid particle numbers. Leach et al. [40] investigated 14 different fuels and several engine conditions. Literature [17,42,43] shows that fuels' propensity to generate soot grows from alkanes to aromatics, with aromatics being the most prone to cause high PN.

There is also evidence that oil characteristics can affect emissions. Kittelson et al. [44] showed how sulfur content had an impact on nanoparticle formation. Wihersaari et al. and Pirjola et al. [45,46] saw that zinc additives also affected overall emissions. Volatility was seen to increase oil consumption due to more evaporated oil in the chamber [47,48]. Nonetheless, with higher volatility, more emissions were encountered by Wihersaari et al. [45] and Lensch-Franzen et al. [49], while viscosity did not have a large impact in these studies. Ash content should be expected to emit more soot as it decreases the oxidation reactivity of particles [50]. This was observed in Zinola et al. [51], where a higher ash content oil slightly increased emissions, and above all, it increased the sub-23 nm particle fraction.

This work focuses specifically on sub-23 nm particle emissions from various oils under steady-state conditions, in contrast to the majority of existing literature, which primarily examines oils' effects on total particle number (TPN) during transient driving cycles [45,46,51–54]. This is part of a project investigating emissions from lubricant oils in decarbonised engine platforms ($H_2$ and $NH_3$) with a focus on emitted particles below

the 23 nm threshold. The overall aim is to assess the viability of new/decarbonised fuels, selecting the most suitable candidate for zero emissions, including the particulate matter, often neglected in $H_2/NH_3$ engines. The next step will then be to test the different oil formulations in the decarbonised platforms to remove the effect of the carbon-based fuel.

## 2. Experimental

For the experimental work of this analysis, a three-cylinder 1.0 litre Ford Ecoboost GDI engine was run with three different oil formulations. A Froude Consine EC38 TA Eddy-Current dynamometer with a rated power of 154 kW was attached to the engine power shaft to measure its torque. The Bosch MED17 engine control unit (ECU) was used to manage spark and injection timing (manufacturer calibration was employed for mapping). At the start of experiments, the engine was run up to 20 Nm-1750 rpm until the oil temperature reached 85 °C. Then, the engine was operated at three torque-speed reference points. These were run at the start and at the end of each testing day to ensure engine running was consistent and that the eventual change in results was not affected by the unexpected alteration of engine parameters. The overall engine specification is shown in Table 2. The engine test setup is represented in Figure 1. All tests were performed on EN228 [55] gasoline fuel with an anti-fouling additive intended to maintain clean injectors and thus minimise the impact of injector fouling on PN as the study progressed.

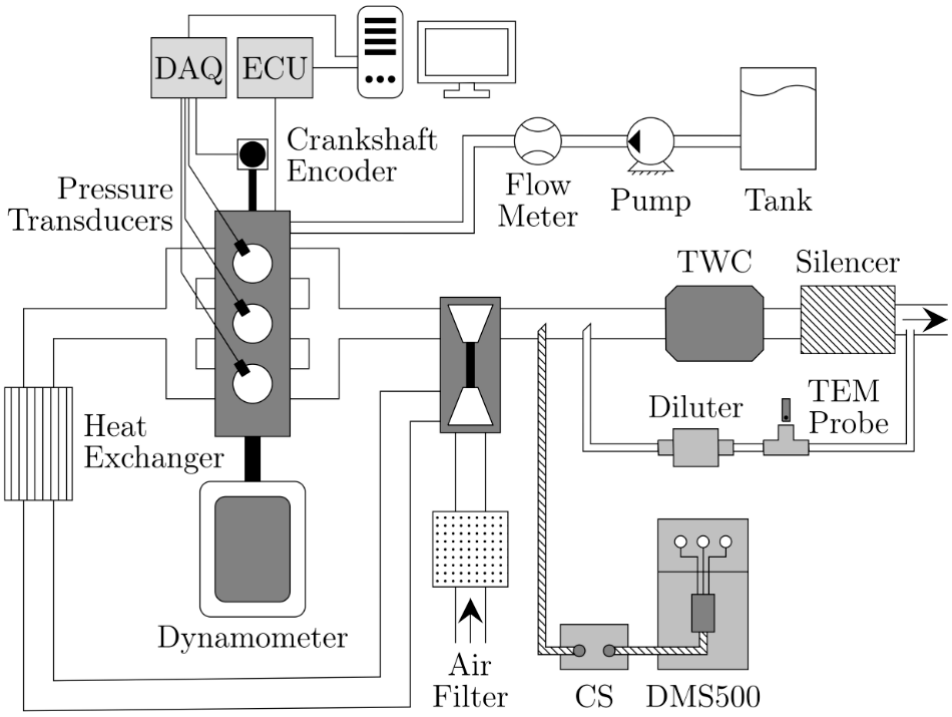


**Figure 1.** Test rig set-up schematic.

Steady-state conditions were investigated with speeds ranging from 1250 rpm to 2250 rpm (in 250 rpm steps) and loads from idle to 40 Nm (in 20 Nm steps). These were chosen to reflect the operating points of the World Harmonised Light Vehicles Test Cycles (WLTC) to be congruous with Euro 6c vehicle testing [56]. The oils tested were:

- 0 W–16, low volatility, low ash "bookend"—(LoLo)
- 0 W–16, high volatility, high ash "bookend"—(HiHi)
- 0 W–20, mid-ash baseline—(Baseline)

In Table 3 a summary of the oil formulations is also included.

**Table 2.** GDI Ford Ecoboost specifications.

| Variable | Value |
|---|---|
| Max. Torque | 170 Nm @ 1400–4500 rpm |
| Max. Power | 92 kW @ 6000 rpm |
| Stroke | 82.0 mm |
| Bore | 71.9 mm |
| Compression ratio (CR) | 10.5:1 |
| Volume | 999 $cm^3$ |
| Injector | 5-hole solenoid |
| Max. Injection Pressure | 200 bar (common rail) |

**Table 3.** Oil formulation summary.

| ASTM | Parameter | LoLo (0–16 W) | Baseline (0–20 W) | HiHi (0–16 W) |
|---|---|---|---|---|
| D2270 [57] | KV at 40 °C $mm^2/s$ | 39.2 | 41 | 38 |
| D4683 [58] | KV at 100 °C $mm^2/s$ | 7.7 | 8.1 | 7.7 |
| D5293 [59] | HTHS (cP) | 2.5 | 2.6 | 2.5 |
| D5800 [60] | Noack (%) | 12 | 11.2 | 30.2 |
| Calculated | Sulfated ash (%) | 0.6 | 0.8 | 1.4 |

The first two oils are expected to define, respectively, the lowest and the highest emission limits, while the baseline is used as a mid-limit reference. To ensure that residual oil, soot, and wear were removed, a cleaning procedure was followed. This comprised two rounds of flushing with the new engine oil combined with a brief steady-state engine run each to ensure the entire oil circuit was cleared. With the third and final filling of the new oil, 10 h of steady-state running was conducted to break in the oil.

The sampling of the exhaust was performed with a Cambustion DMS500 for particulate measurements. The 5 m heated line and the sampling block were run at 191 °C. The 1000 nm mode was selected to operate the instrument to acquire particles ranging between 5 and 1000 nm. Only the 5:1 primary dilution was adopted, bypassing the second one. The latter was employed 12–250:1 only for 1250 rpm and 1500 rpm fast idling, achieving a better signal strength. The VPR equipped for these experiments was a CS by Cambustion, which had a 99% removal efficiency for 30 nm tetracontane. This was placed in line with the DMS and the heated sampling line (HSL) with cooler and heater temperatures set respectively at 80 °C and 410 °C. A 180 s measurement window was implemented with a 0.5 Hz sampling rate. In addition, a penetration efficiency model by Cambustion was employed, which was also pursued in other research studies [41,61]. This penetration model was executed considering the CS and heated sampling line particle losses and correcting them.

In addition to obtaining the TPN from the PSDs, DFs from Equations (1) and (2) were applied to the raw PSDs to obtain "filtered" PSDs. From the "filtered" PSDs, a "filtered" TPN could be obtained. The same digital filter terminology introduced by Pfau et al. [37] is utilised here for the "filtered" TPNs, and these are "F1-PN > 23" for filtering as per Leach [35] with Equation (1) using d50 = 23 nm and d90 = 41 nm and F3-PN > 10 for filtering as per Pfau [37] with Equation (2) using d65 = 10 nm and d90 = 15 nm.

## 3. Results and Discussion

First, the DMS500 without CS was used to analyse PSDs on the GDI engine. The digital filtering approach by Leach [35] (1) was then implemented on the raw PSDs to obtain F1-PN > 23 [35]. Subsequently, PSDs were measured again, this time using the catalytic stripper. Equation (2) by Pfau et al. [37] was applied to obtain F3-PN > 10 [37] from the new raw PSDs. F1-PN > 23 and F3-PN > 10 for the baseline, LoLo and HiHi oils are shown in Figure 2.

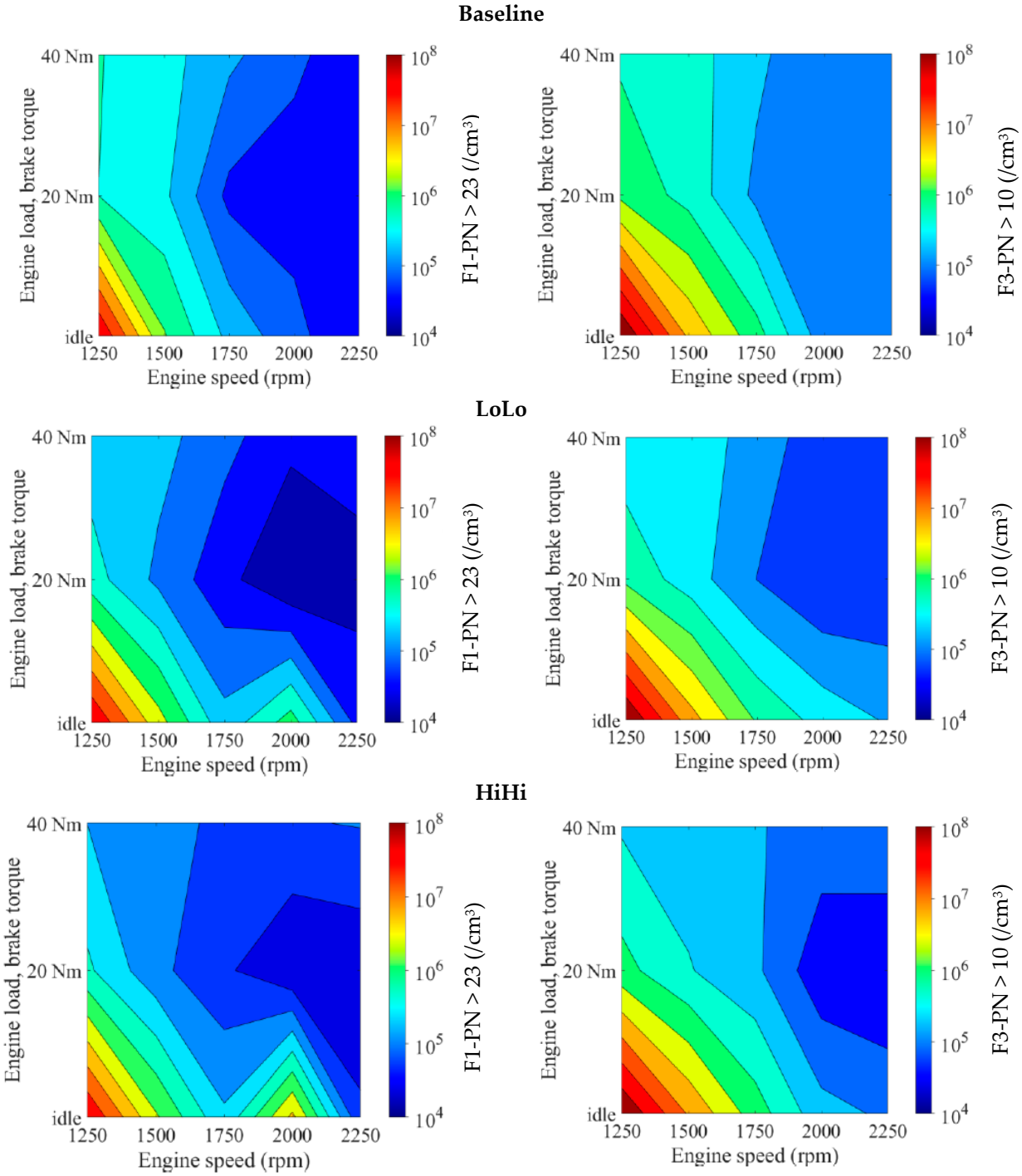


**Figure 2.** Baseline, LoLo, and HiHi SPN with F1-PN > 23 and F3-PN > 10.

Both LoLo and HiHi exhibit F1-PN > 23 concentration levels that are generally lower than baseline oil, especially at medium-high loads for all speed ranges. In contrast, they are higher at all speeds of idling. A similar outcome is found in F3-PN > 10 with LoLo and HiHi emissions only exceeding baseline at fast idle and at 2250 rpm-40 Nm. This result is better emphasised and represented in the comparison contour graphs in Figure 3, where the percentage difference in filtered PNs of baseline to LoLo and to HiHi is directly plotted by overlapping Figure 2 images. This indicates that the baseline has a greater PN relative to either LoLo or HiHi when a red shade colour is present (positive percentage), whereas a green shade colour indicates the opposite. Also, in the figure, the tables display the percentage differences in the contour plots at each of the selected test matrix points.

These plots make it easier to see how the two oils have lower F1-PN > 23 and F3-PN > 10 than baseline at multiple points. The baseline has reduced emissions mostly at fast idle and 2250 rpm-40 Nm.

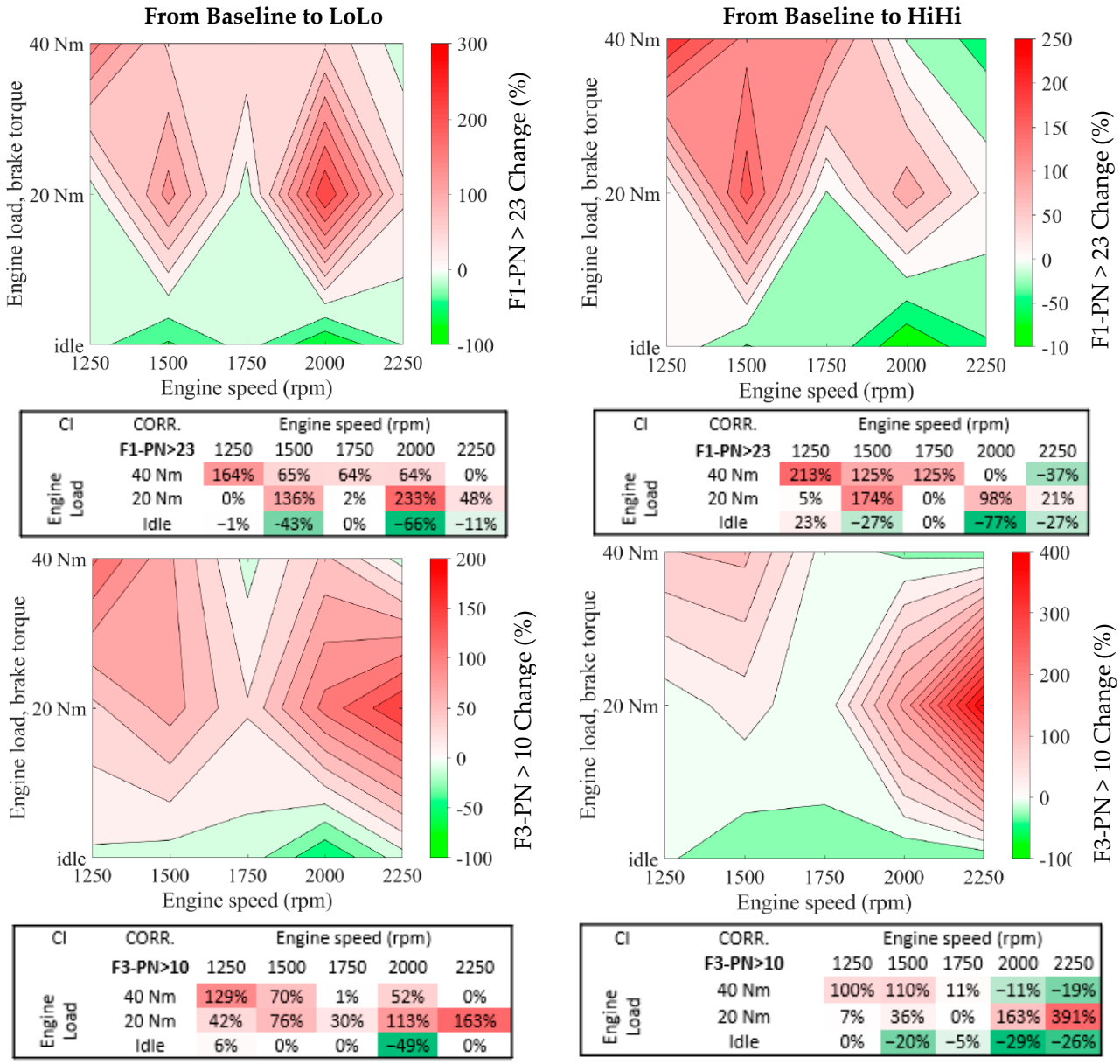


**Figure 3.** F1-PN > 23 and F3-PN > 10 Baseline to LoLo and HiHi comparison plots.

Furthermore, a direct percentage difference of HiHi relative to LoLo is also performed and depicted in Figure 4. HiHi confirms a higher F1-PN > 23 level at mid-high speeds for all loads. This changes for F3-PN > 10, where HiHi has a lower count in the region between 2000 rpm-fast idle and 2250 rpm-20 Nm, except at 2250 rpm-fast idle. Variation ranges from −22% to +289% in F1-PN > 23 and from −34% to 104% in F3-PN > 10. To condense the PN differences in a single value, a weighted arithmetic mean (WAM) was calculated while accounting for the confidence interval (CI) correction. According to this, HiHi's overall F1-PN > 23 was 9.7% higher than LoLo, and its F3-PN > 10 was 3.6% higher than LoLo.

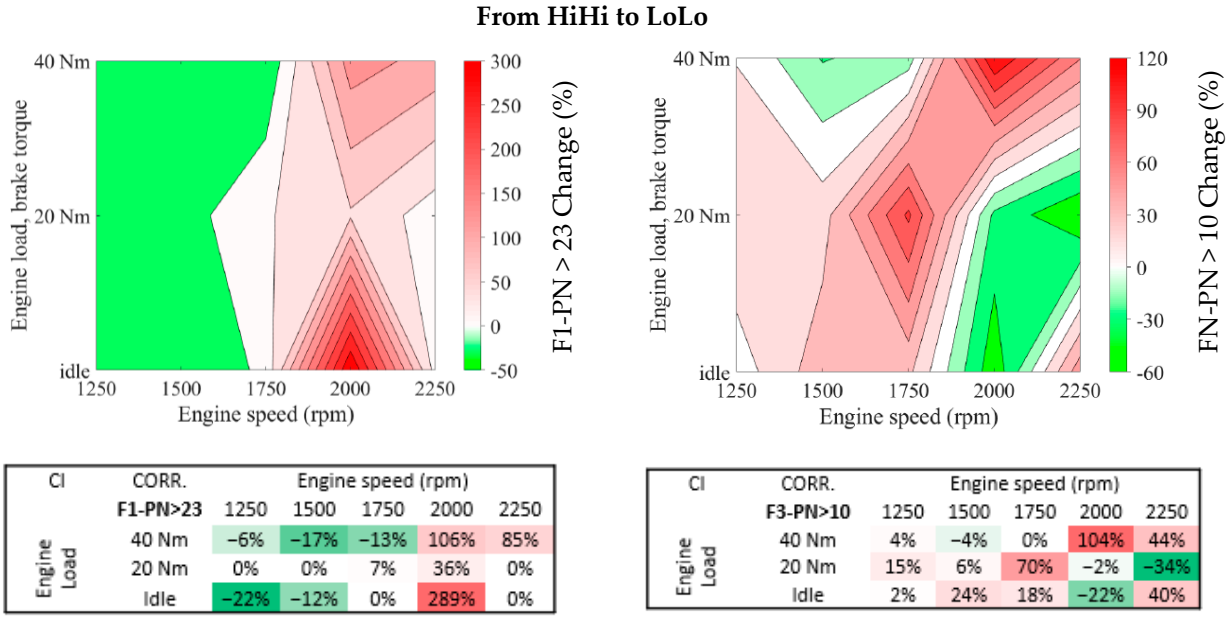


| CI | CORR. | Engine speed (rpm) | | | | |
|---|---|---|---|---|---|---|
| | **F1-PN>23** | 1250 | 1500 | 1750 | 2000 | 2250 |
| Engine Load | 40 Nm | −6% | −17% | −13% | 106% | 85% |
| | 20 Nm | 0% | 0% | 7% | 36% | 0% |
| | Idle | −22% | −12% | 0% | 289% | 0% |

| CI | CORR. | Engine speed (rpm) | | | | |
|---|---|---|---|---|---|---|
| | **F3-PN>10** | 1250 | 1500 | 1750 | 2000 | 2250 |
| Engine Load | 40 Nm | 4% | −4% | 0% | 104% | 44% |
| | 20 Nm | 15% | 6% | 70% | −2% | −34% |
| | Idle | 2% | 24% | 18% | −22% | 40% |

CI Corrected F1-PN > 23 Difference:

- Mean: 30.2% (raw 37.5%)
- **WAM: 9.7%**

CI Corrected F3-PN > 10 Difference:

- Mean: 17.7% (raw 23.6%)
- **WAM: 3.6%**

**Figure 4.** F1-PN > 23 and F3-PN > 10 HiHi to LoLo comparison plots.

High ash and volatility emitting more PN have also been detected in other research work. Easter et al. [50] show that higher ash content is expected to decrease the oxidation reactivity of soot particles, leading to a higher particle count due to less soot being lost through oxidation. Zinola et al. [51] found not only slightly higher emissions with higher ash but also a higher sub-23 nm proportion being formed. Lenschen-Franzen et al. [49] observed a 5% increase in particle number emission from exhaust (measured using DMS) with Noack volatility from 8% to 19% over eight medium power points. Wihersaari et al. [45] learnt similar results using three different oil formulations. The two oils with higher Noack volatility had higher soot emissions, except in the <30 nm region, where the low volatility oil had more particles in steady-state driving cycles. This overall trend of higher volatility increasing emissions could be due to an increase in oil consumption—a relationship supported by past research [47,48]. The way volatility can affect consumption can be due to its direct effect on oil evaporation. The oil evaporation mechanism from the cylinder wall occurs as the piston rings deposit during the downward stroke a thin oil film on the surface. Over the combustion, high temperatures cause the oil to vaporise and mix with the combustion gases, particularly in the power and exhaust strokes [49]. In modern engines with low oil consumption, only a few molecular layers of oil are lost per cycle, influenced by pressure, temperature, gas velocity, and oil composition. Lubricating oil with higher volatility enables more oil vapour into the combustion chamber. One of the ways in which oil volatility can affect particle formation is with the volatile elements getting condensed or adsorbed onto the particle surface. Volatile hydrocarbon vapours may also nucleate and form new particles. As also found by Miller et al. [62], this depends on the level of volatility, local cooling degree, and concentration. The relative impact also depends on running conditions and fuel mixture [45,49]. Therefore, the outcome of this investigation is consistent with previous research, though the baseline is not exactly in the middle of the spectrum, being even higher than HiHi under some conditions. This would need further investigation of why it occurred. Since higher ash results in even

smaller particles, it may be that these were grown by condensation of more oil on them due to higher volatility, remaining at the end in the same nucleation order. However, it is not clear why at some matrix points HiHi PN is lower than baseline even without the catalytic stripper. This notably shows that the running condition is pivotal in causing fewer or more TPN emissions. To further verify this, a three-way ANOVA was performed (Tables 4 and 5). This is a robust method for determining what has the most statistically significant impact on the emissions. The observed data were F1 PN > 23 (Table 4) and F1 PN > 10 (Table 5) for all 15 conditions. Below are the summary tables, where "Source" is the factor or interaction being analysed and "DoF" are the degrees of freedom from the number of independent variables contributing to the variance. Oil type, load, and speed were chosen as independent variables. The tables show that for the overall 15 steady-state conditions, load and speed are the dominant factors impacting the TPN emissions. The same was repeated for raw TPN, obtaining the same result. However, individual test points still show a significant impact of oil formulation as per Figures 3 and 4.

**Table 4.** Summary ANOVA F1 PN > 23.

| Source | DoF | Sum of Squares | Mean Square | F-Statistic | *p*-Value |
|---|---|---|---|---|---|
| Oil Type | 2 | $1.34 \times 10^{13}$ | $6.70 \times 10^{12}$ | 0.03 | 0.971 |
| Load (Nm) | 2 | $2.39 \times 10^{15}$ | $1.19 \times 10^{15}$ | 5.19 | 0.01 |
| Speed (rpm) | 4 | $4.13 \times 10^{15}$ | $1.03 \times 10^{15}$ | 4.48 | 0.005 |
| Error | 36 | $8.29 \times 10^{15}$ | $2.30 \times 10^{14}$ | | |
| Total | 44 | $1.48 \times 10^{16}$ | | | |

**Table 5.** Summary ANOVA F3 PN > 10.

| Source | DoF | Sum of Squares | Mean Square | F-Statistic | *p*-Value |
|---|---|---|---|---|---|
| Oil Type | 2 | $2.04 \times 10^{13}$ | $1.02 \times 10^{13}$ | 0.01 | 0.994 |
| Load (Nm) | 2 | $1.86 \times 10^{16}$ | $9.30 \times 10^{15}$ | 5.15 | 0.011 |
| Speed (rpm) | 4 | $3.32 \times 10^{16}$ | $8.30 \times 10^{15}$ | 4.59 | 0.004 |
| Error | 36 | $6.51 \times 10^{16}$ | $1.81 \times 10^{15}$ | | |
| Total | 44 | $1.17 \times 10^{17}$ | | | |

Another important aspect to highlight is observing how the F3-PN > 10 difference (3.6%) decreased with respect to the F1-PN > 23 (9.7%) from HiHi to LoLo oil in Figure 4. This could indicate that LoLo is emitting a higher number of <23 nm particles than HiHi. A reasonable explanation may be that high volatility shifts particle size towards a larger diameter as there is a larger quantity of oil vapour that can condense on particles [63] or more simply, the catalytic stripper used in F3-PN > 10 has eliminated more volatiles being formed in HiHi. This can be interpreted by looking at the PSDs plots in Figure 5.

They are equally extracted from the DMS500 for each test condition and oil utilised. The sets of charts from lowest to highest speed (Figure 5) are represented in a grid to visualise the results and compare them to each other more easily. Mean raw PSDs with (w) and without (w/o) CS are plotted together. Confidence intervals are not included for more clarity, but are shown in Appendix A (Figures A1–A3).

The correlation between PSDs and filtered PNs in Figure 3 is evident, as either the baseline or the HiHi has the highest nucleation mode, except at 1250 rpm-idle where all three oils are similar (Figure 5). In addition, the effect of the CS can be noticed, as it eliminates the volatiles in the exhaust gas and shifts all the PSDs towards larger mobility diameters. Also, the PSDs allow verifying that LoLo is not emitting more sub-23 nm than HiHi as could have been thought by the drop in the weighted arithmetic mean previously computed. Since the HiHi oil produces more volatiles and, hence, higher emissions without CS, it typically has a larger nucleation mode, especially around 2250 rpm. This is why HiHi has a higher proportion of sub-23 nm particles than LoLo, with no obvious movement

towards larger diameters. Consequently, as expected, the CS has a greater impact on the HiHi oil than the LoLo and the baseline, significantly lowering its PSD modes between 5 and 10 nm, since most of the volatiles are present in this range.

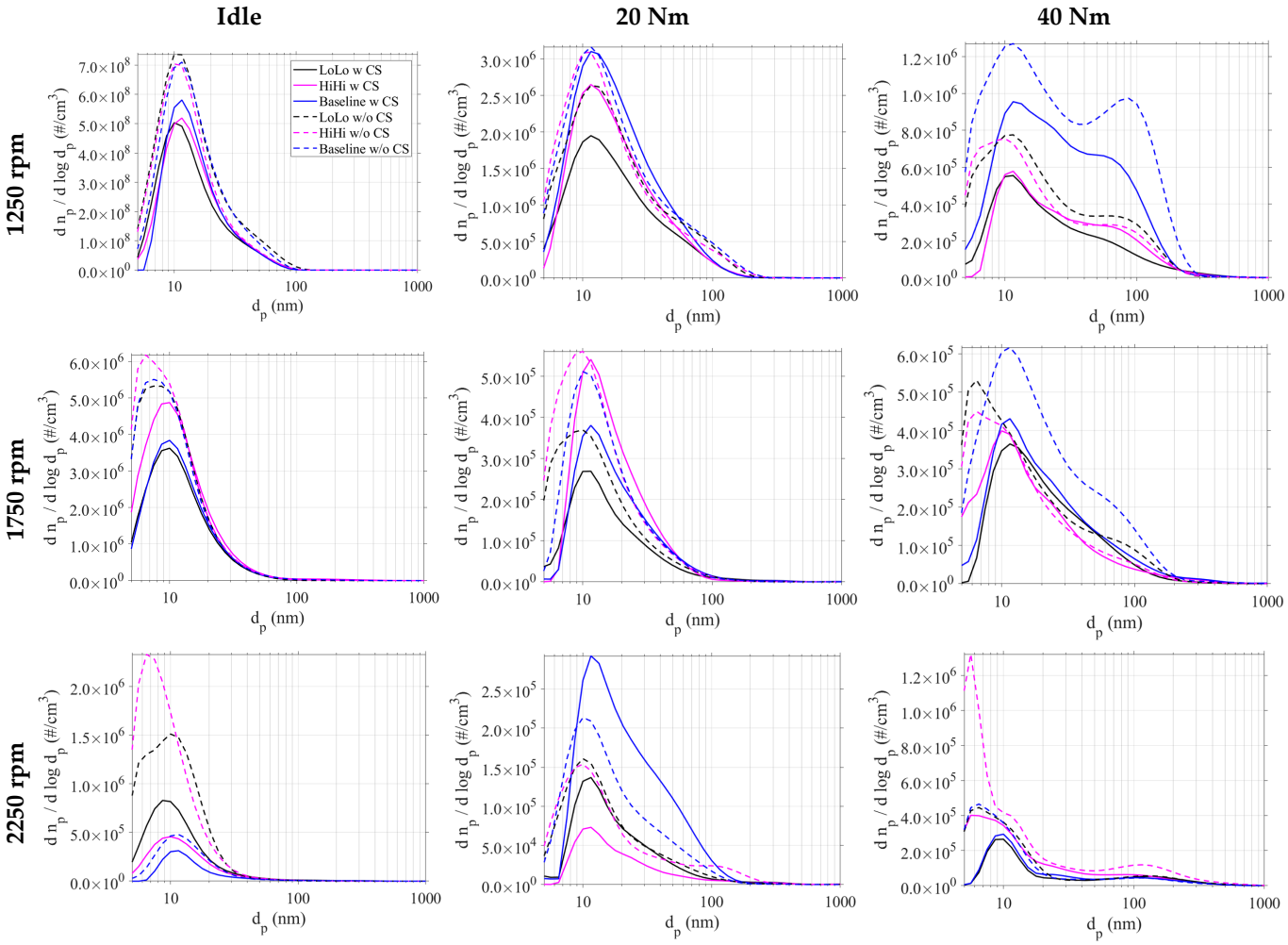


**Figure 5.** Raw PSDs over low, mid, and high-speed conditions. "#" is for "number". Legend in the top left plot, 1250 rpm-idle.

Looking at Figure 5, at 1250 rpm, both LoLo and HiHi show the lowest nucleation modes with CS at approximately $5 \times 10^8/\text{cm}^3$ at idle, respectively, $1.9 \times 10^6/\text{cm}^3$ and $2.6 \times 10^6/\text{cm}^3$ at 20 Nm and $5 \times 10^5/\text{cm}^3$ at 40 Nm. Without CS, their profile is close to the baseline, but at 40 Nm, the accumulation mode is much less pronounced. LoLo has a lower level only at 20 Nm. All graphs show nucleation mode with particle diameters around 10–12 nm.

At 1750 rpm, the baseline is lower than the HiHi oil, except at 40 Nm, where it has a higher nucleation mode. HiHi emits the highest quantity overall at idle with $6 \times 10^6/\text{cm}^3$ w/o CS and $5 \times 10^6/\text{cm}^3$ w CS. All oils present a nucleation mode in an equivalent size range at approximately 8–10 nm at idle, 10–13 nm at 20 Nm, and 6.5–12 nm at 40 Nm.

Finally, at 2250 rpm, the baseline has low concentration levels below $5 \times 10^5/\text{cm}^3$ (again remaining consistent with Figure 3). Only 20 Nm has the highest emissions among the oils. HiHi has the highest emissions at idle and 40 Nm. At this speed, its PSD profile is different from the baseline, unlike the previous results, where they were more analogous.

The raw PSDs made it possible to comprehend the size range of PN emissions with speed and load conditions, as well as to see the functioning of the digital filters. Leach

et al. [48], similarly, utilised the PSDs to determine what the DF was discounting from the TPN produced by 10 different fuels. In doing so, particles that the DMS500 had identified in the raw PSDs were effectively eliminated. This impact may be seen in Figure 4 when comparing F1-PN > 23 and F3-PN > 10. In Pfau et al. [36], the comparison between different DF approaches showed in detail how results could vary depending on which one was employed. Overall, it is evident that PSDs are fundamental to estimating the sub-23 nm fraction and assessing their contribution to the PN emissions. The most important finding in this study is that the three oil formulations did not alter the nucleation mode diameter in the PSDs. Changes occurred only in terms of filtered PNs at specific conditions, while the nucleation mode diameter shift was caused only by the CS due to the burning of volatiles. This disagrees with the hypothesis that more oil vapour from high-volatility oils is expected to condense on particles, making them larger.

## 4. Conclusions

The PN emissions of three different oil formulations were examined in a 1.0 L gasoline direct injection engine under 15 steady-state load and speed conditions. Unlike most studies that focus on transient driving cycles, this research investigates oil impact on total particulate number (TPN) emissions under stable operating conditions, with particular emphasis on sub-23 nm particles. To simulate the detection efficiency of a condensation particle counter, two digital filters were applied to the raw PN data from a DMS500. F1-PN > 23 had a detection efficiency of d50 = 23 nm and d90 = 41 nm, while F3-PN > 10 had a detection efficiency of d50 = 10 nm and d90 = 15 nm. The three tested oil formulations included a mid-ash baseline, a low-ash low-volatility (LoLo) formulation, and a high-ash high-volatility (HiHi) formulation. The main findings included:

- Depending on the condition, the baseline oil exhibited higher PN emissions with both digital filters, except at low loads. LoLo generally produced the lowest PN. Using the weighted arithmetic mean, HiHi had a higher F1-PN > 23 than LoLo by 9.7%, while F3-PN > 10 was higher by 3.6%.
- Over the full test matrix, a three-way ANOVA analysis revealed that load and speed were the dominant factors influencing TPN emissions. However, under specific conditions, the impact of oil on particulates is still clear and relevant.
- Particle size distributions (PSDs) and filtered PNs showed that HiHi had a higher sub-23 nm fraction than LoLo due to its greater volatile content. All PSD nucleation modes were observed around 8–12 nm, confirming that most emissions were in the sub-23 nm region.
- Oil formulation did not significantly impact the nucleation mode diameter of PSDs, as no lateral shift in the distributions was observed. However, nucleation modes shifted to larger diameters when the catalytic stripper was used, as it effectively removed volatile particles in the 5–10 nm region.

In conclusion, this study highlights the critical need for further research on oil-related particulate emissions under steady-state conditions, particularly for sub-23 nm particles, as upcoming Euro 7 regulations tighten measurement thresholds to 10 nm, and emphasises the importance of exploring non-carbon fuels like ammonia ($NH_3$) or hydrogen ($H_2$) to fully understand the real impact of oils on particulate emissions.

**Author Contributions:** Conceptualization, S.A.P.; methodology, S.A.P.; software, S.A.P.; investigation, S.A.P. and E.H.-S.; data curation, S.A.P.; formal analysis, S.A.P. and S.L.; validation, S.A.P. and S.L.; visualization, S.A.P. and S.L.; writing—original draft, S.L. and E.H.-S.; writing—review and editing S.L., S.A.P., E.H.-S. and A.L.R.; supervision, A.L.R. and A.C.; funding acquisition, A.L.R. All authors have read and agreed to the published version of the manuscript.

**Funding:** This work was supported by the Engineering and Physical Sciences Research Council through the scholarship provided by EPSRC for Salvatore Lagana [grant number EP/T517902/1].

**Institutional Review Board Statement:** Not applicable.

**Informed Consent Statement:** Not applicable.

**Data Availability Statement:** The raw data supporting the conclusions of this article will be made available by the authors on request.

**Acknowledgments:** The authors thank John Lane and Nigel Sykes for their technical support with the engine setup. The authors further thank Lubrizol Limited for funding and supply of the fuel and lubricating oils.

**Conflicts of Interest:** The authors declare no conflicts of interest.

## Abbreviations

The following abbreviations are used in this manuscript:

| | |
|---|---|
| WAM | Weighted arithmetic mean—this accounted for the confidence intervals in the calculation of the mean. |
| HiHi | High ash high volatility formulation |
| LoLo | Low ash low volatility formulation |
| PN | Particle number |
| TPN | Total particle number—this includes solid and volatile particles. |
| CS | Catalytic stripper |
| DMS | Differential mobility spectrometer |
| PSD | Particle size distribution |
| CPC | Condensation particle counter |
| d50 = 23 nm | Naming convention to indicate that only 50% of particles with 23 nm in size can be detected. This refers to the detection efficiency of condensation particle counters. |
| SPN | Solid particle number—TPN after a VPR is applied, like a catalytic stripper. |
| SPN23 | Standard detection efficiency method counting "Solid Particle Number" with 50% efficiency at 23 nm (d50 = 23 nm) and 90% at 41 nm (d90 = 41 nm). This is currently used by PMP with Euro 6. |
| Sub-23 nm | Particles under 23 nm in diameter |
| SPN10 | New proposed standard detection efficiency method counting "Solid Particle Number" with 65 $\pm$ 15% efficiency at 10 nm (d65 = 10 nm) and 90% at 15 nm (d90 = 15 nm). This should be in Euro 7 from 2025. |
| Sub-10 nm | Particles under 10 nm in diameter |
| DF | Digital filter. This applies prescribed counting efficiency to discount from a DMS the particles from a raw PSD diagram. This allows comparison of DMS data to a condensation particle counter. |
| F1-PN > 23 | Digital filter with detection efficiency of d50 = 23 nm and d90 = 41 nm, this is the PN derived from the DMS PSDs without the catalytic stripper. |
| F3-PN > 10 | Digital filter with detection efficiency of d65 = 10 nm and d90 = 15 nm, this is the PN derived from the DMS PSDs with the catalytic stripper. |
| dp | Particle diameter |

## Appendix A

PSDs with confidence intervals are shown here.

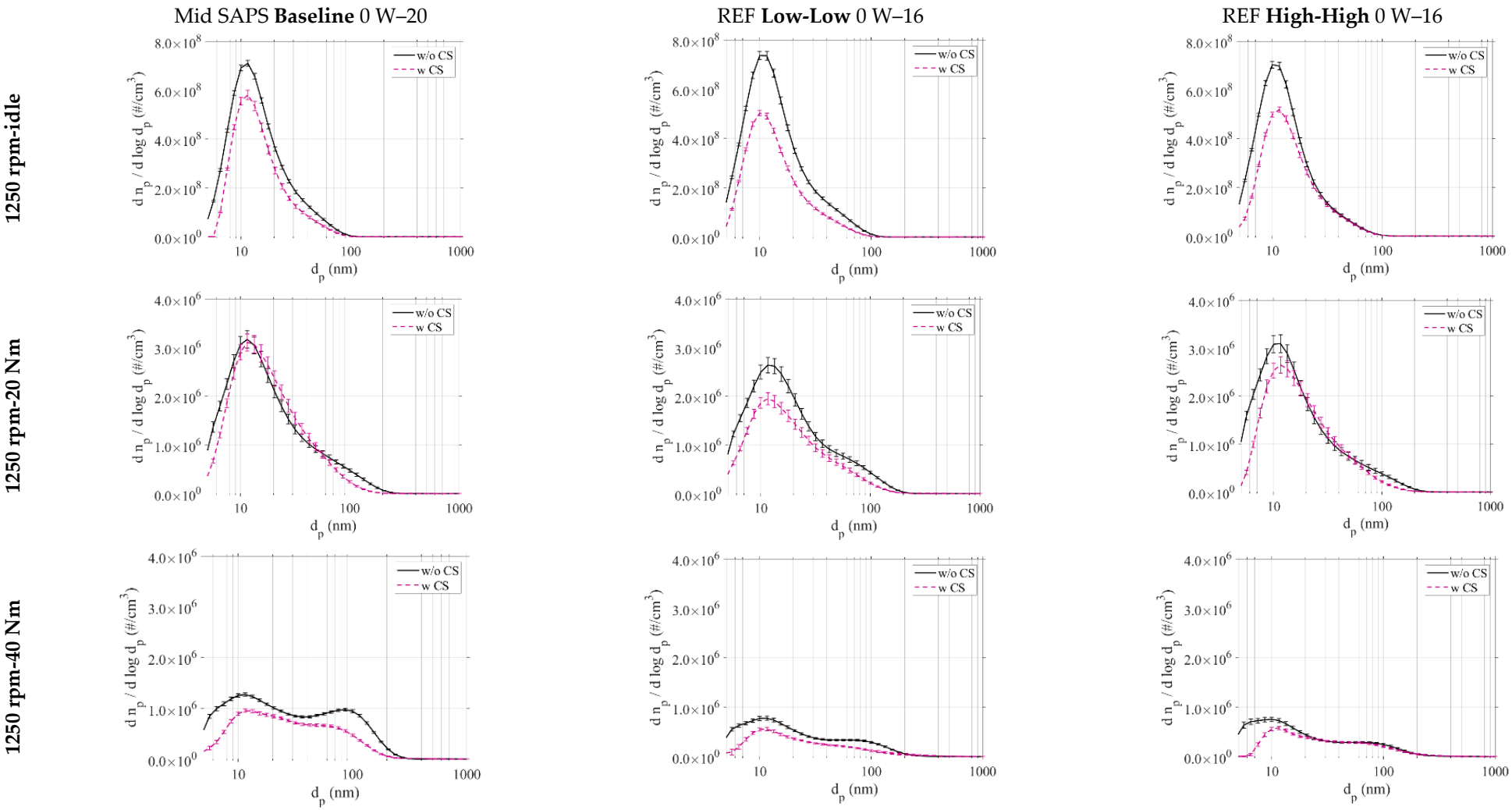


**Figure A1.** PSD at 1250 rpm-varying Load. "#" is for "number".

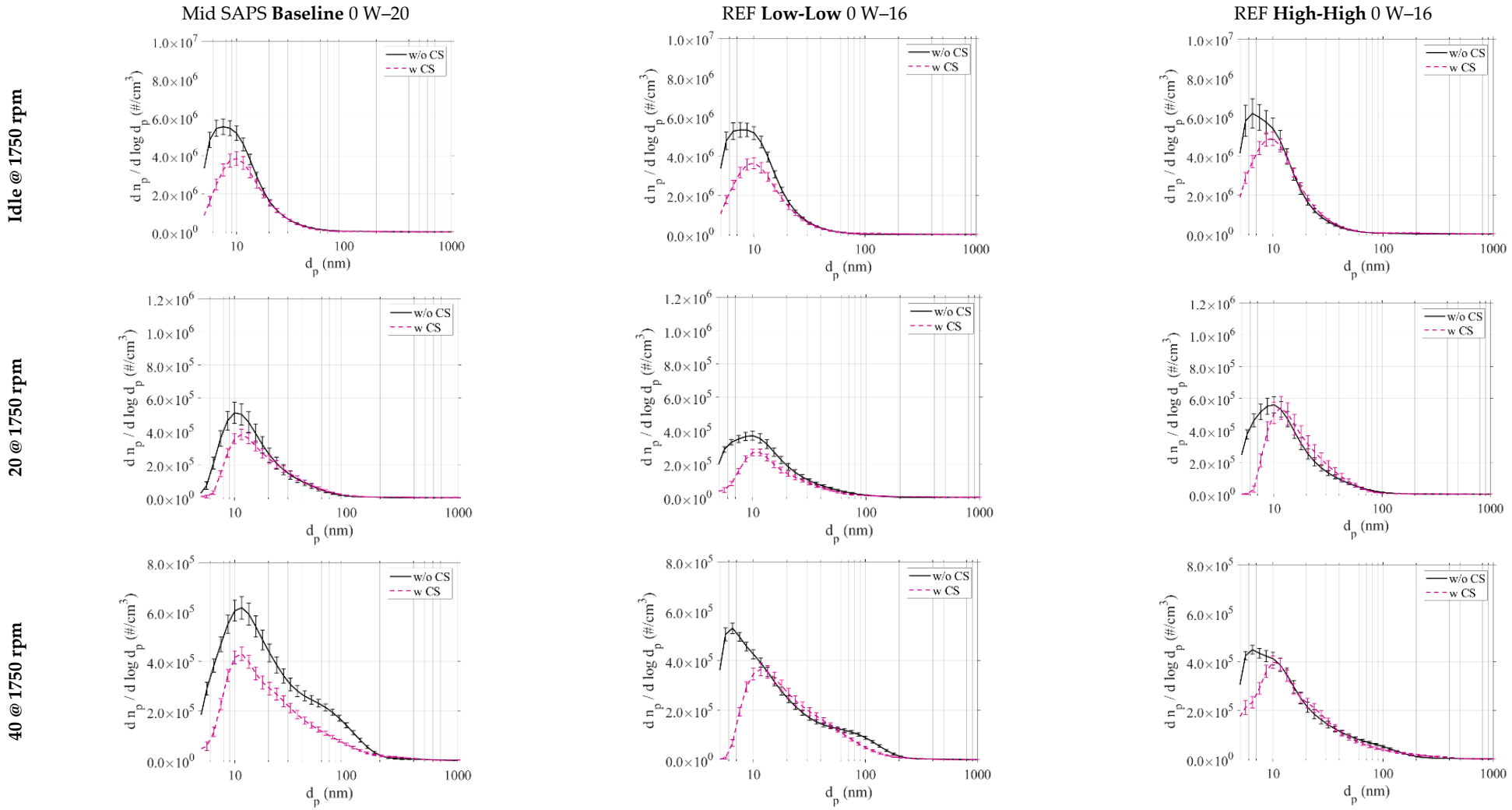


**Figure A2.** PSD at 1750 rpm-varying Load. "#" is for "number".

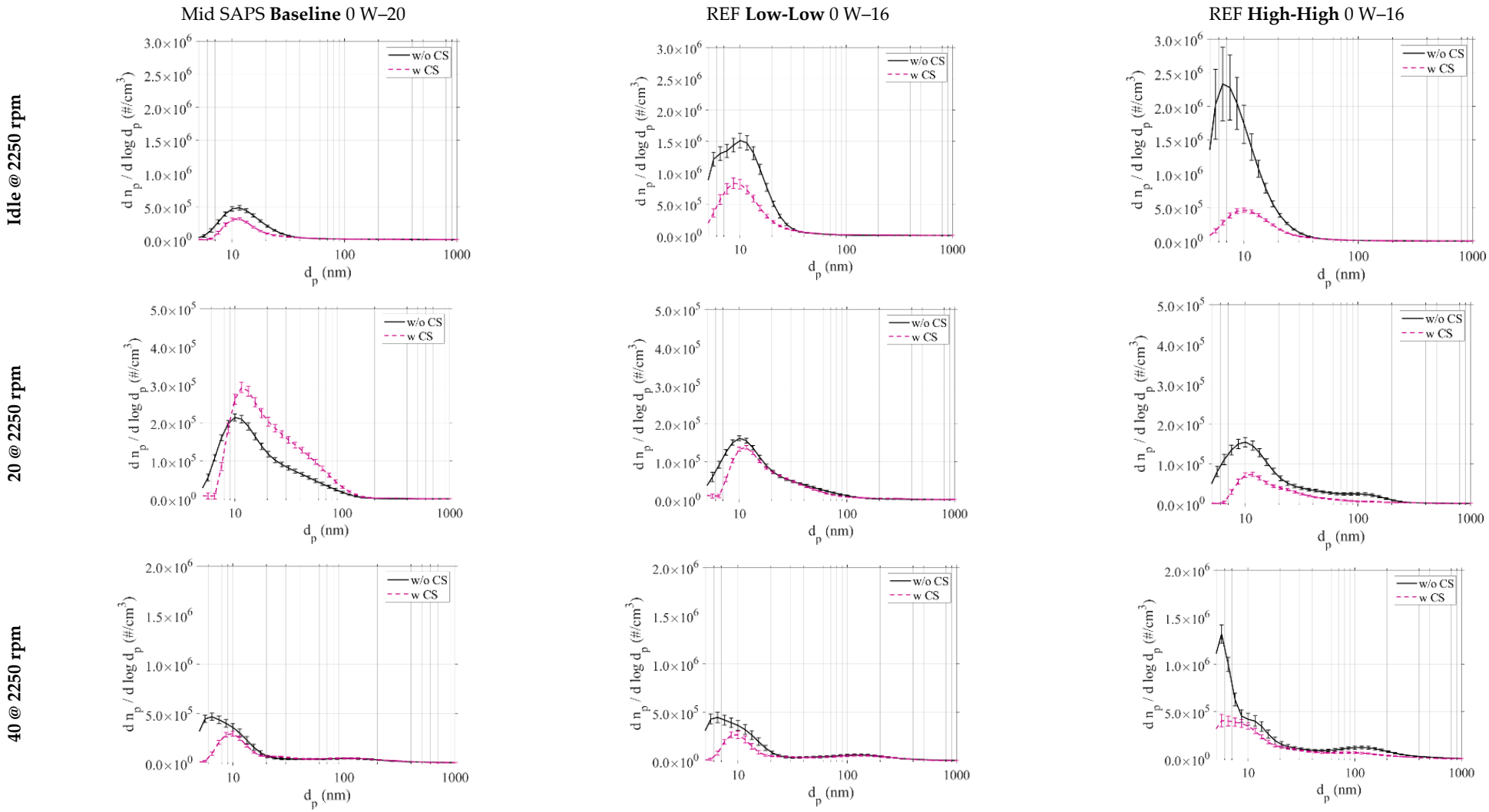


**Figure A3.** PSD at 2250 rpm-varying Load. "#" is for "number".

## References


1. Health Effects Institute. *State of Global Air 2018*; Health Effects Institute: Boston, MA, USA, 2018. Available online: https://www.stateofglobalair.org/sites/default/files/soga-2018-report.pdf (accessed on 4 October 2022).
2. World Health Organization. *Ambient Air Pollution: A Global Assessment of Exposure and Burden of Disease*; World Health Organization: Geneva, Switzerland, 2016. (In English)
3. US Environmental Protection Agency (EPA). Health and Environmental Effects of Particulate Matter (PM). Available online: https://www.epa.gov/pm-pollution/health-and-environmental-effects-particulate-matter-pm (accessed on 4 October 2022).
4. Health Effects Institute. *The State of Global Air 2024*; Health Effects Institute: Boston, MA, USA, 2024. Available online: https://www.healthdata.org/sites/default/files/2024-06/soga-2024-report.pdf (accessed on 10 January 2025). (In English)
5. Oberdörster, G.; Sharp, Z.; Atudorei, V.; Elder, A.; Gelein, R.; Kreyling, W.; Cox, C. Translocation of inhaled ultrafine particles to the brain. *Inhal Toxicol* **2004**, *16*, 437–445. [CrossRef] [PubMed]
6. Schraufnagel, D.E.; Balmes, J.R.; Cowl, C.T.; De Matteis, S.; Jung, S.-H.; Mortimer, K.; Perez-Padilla, R.; Rice, M.B.; Riojas-Rodriguez, H.; Sood, A.; et al. Air Pollution and Noncommunicable Diseases: A Review by the Forum of International Respiratory Societies' Environmental Committee, Part 2: Air Pollution and Organ Systems. *Chest* **2019**, *155*, 417–426. [CrossRef]
7. Schraufnagel, D.E. The health effects of ultrafine particles. *Exp. Mol. Med.* **2020**, *52*, 311–317. [CrossRef]
8. Stocker, T.F.; Qin, D.; Plattner, G.-K.; Tignor, M.; Allen, S.K.; Boschung, J.; Nauels, A.; Xia, Y.; Bex, V.; Midgley, P.M. *Climate Change 2013: The Physical Science Basis. Contribution of Working Group I to the Fifth Assessment Report of the Intergovernmental Panel on Climate Change*; IPCC: Cambridge, UK; New York, NY, USA, 2013; p. 1535. Available online: https://www.ipcc.ch/site/assets/uploads/2018/03/WG1AR5_SummaryVolume_FINAL.pdf (accessed on 4 October 2022).
9. Aamaas, B.; Lund, M.T.; Myhre, G.; Samset, B.H.; Stjern, C.W.; Kallbekken, S. The climate impacts of current black carbon and organic carbon emissions. *CICERO Rep.* **2018**. Available online: http://hdl.handle.net/11250/2502504 (accessed on 4 October 2022).
10. Climate and Clean Air Coalition (CCAC). Climate and Clean Air Coalition (CCAC)—Black Carbon. Available online: https://www.ccacoalition.org/en/slcps/black-carbon (accessed on 4 October 2022).
11. Jacobson, M.Z. Control of fossil-fuel particulate black carbon and organic matter, possibly the most effective method of slowing global warming. *J. Geophys. Res. Atmos.* **2002**, *107*, ACH 16-11–ACH 16-22. [CrossRef]
12. Wappelhorst, S. *Update on Government Targets for Phasing Out New Sales of Internal Combustion Engine Passenger Cars*; International Council on Clean Transportation (ICCT): Washington, DC, USA, 2021. Available online: https://theicct.org/wp-content/uploads/2021/12/update-govt-targets-ice-phaseouts-jun2021_0.pdf (accessed on 10 September 2024).
13. Krajinska, A. *Euro 7: Europe's Chance to Have Clean Air*; Transport and Environment: Brussels, Belgium, 2021. Available online: https://www.transportenvironment.org/discover/euro-7-europes-chance-to-have-clean-air/ (accessed on 4 October 2022).
14. Heywood, J.B. *Internal Combustion Engine Fundamentals*, 2nd ed.; McGraw-Hill Education: New York, NY, USA, 2018. (In English)
15. La Rocca, A.; Bonatesta, A.F.; Fay, M.W.; Campanella, F. Characterisation of soot in oil from a gasoline direct injection engine using Transmission Electron Microscopy. *Tribol. Int.* **2015**, *86*, 77–84. [CrossRef]
16. Shuai, S.; Ma, X.; Li, Y.; Qi, Y.; Xu, H. Recent Progress in Automotive Gasoline Direct Injection Engine Technology. *Automot. Innov.* **2018**, *1*, 95–113. [CrossRef]
17. Flagan, R.C.; Seinfeld, J.H. *Fundamentals of Air Pollution Engineering*; Courier Corporation: North Chelmsford, MA, USA, 2012.
18. Shao, C.; Wang, Q.; Zhang, W.; Bennett, A.; Li, Y.; Guo, J.; Im, H.G.; Roberts, W.L.; Violi, A.; Sarathy, S.M. Elucidating the polycyclic aromatic hydrocarbons involved in soot inception. *Commun. Chem.* **2023**, *6*, 223. [CrossRef]
19. Richter, H.; Howard, J.B. Formation of polycyclic aromatic hydrocarbons and their growth to soot—A review of chemical reaction pathways. *Prog. Energy Combust. Sci.* **2000**, *26*, 565–608. [CrossRef]
20. Kittelson, D.; Kraft, M. *Particle Formation and Models*; John Wiley & Sons Ltd.: Hoboken, NJ, USA, 2014; pp. 1–23. [CrossRef]
21. Mansurov, Z.A. Formation of soot from polycyclic aromatic hydrocarbons as well as fullerenes and carbon nanotubes in the combustion of hydrocarbon. *J. Eng. Phys. Thermophys.* **2011**, *84*, 125–159. [CrossRef]
22. Hou, D.; Pascazio, L.; Martin, J.; Zhou, Y.; Kraft, M.; You, X. On the reactive coagulation of incipient soot nanoparticles. *J. Aerosol Sci.* **2022**, *159*, 105866. [CrossRef]
23. Michelsen, H.A.; Colket, M.B.; Bengtsson, P.-E.; D'Anna, A.; Desgroux, P.; Haynes, B.S.; Miller, J.H.; Nathan, G.J.; Pitsch, H.; Wang, H. A Review of Terminology Used to Describe Soot Formation and Evolution under Combustion and Pyrolytic Conditions. *ACS Nano* **2020**, *14*, 12470–12490. [CrossRef] [PubMed]
24. Omidvarborna, H.; Kumar, A.; Kim, D.-S. Recent studies on soot modeling for diesel combustion. *Renew. Sustain. Energy Rev.* **2015**, *48*, 635–647. [CrossRef]
25. Joint Research Centre Institute for Energy Transport; Mamakos, A.; Martini, G.; Dardiotis, C. *Assessment of Particle Number Limits for Petrol Vehicles*; Publications Office: Luxembourg, 2012. [CrossRef]
26. Jonson, J.E.; Borken-Kleefeld, J.; Simpson, D.; Nyíri, A.; Posch, M.; Heyes, C. Impact of excess $NO_x$ emissions from diesel cars on air quality, public health and eutrophication in Europe. *Environ. Res. Lett.* **2017**, *12*, 094017. [CrossRef]

27. Williams, M.; Minjares, R. *A Technical Summary of Euro 6/VI Vehicle Emission Standards*; International Council on Clean Transportation (ICCT): Washington, DC, USA, 2016. Available online: https://theicct.org/sites/default/files/publications/ICCT_Euro6-VI_briefing_jun2016.pdf (accessed on 4 October 2022).
28. Giechaskiel, B.; Woodburn, J.; Szczotka, A.; Bielaczyc, P. Particulate Matter (PM) Emissions of Euro 5 and Euro 6 Vehicles Using Systems with Evaporation Tube or Catalytic Stripper and 23 nm or 10 nm Counters. In Proceedings of the SAE Powertrains, Fuels & Lubricants Meeting, Krakow, Poland, 22–23 September 2020. [CrossRef]
29. Giechaskiel, B.; Mamakos, A.; Andersson, J.; Dilara, P.; Martini, G.; Schindler, W.; Bergmann, A. Measurement of Automotive Nonvolatile Particle Number Emissions within the European Legislative Framework: A Review. *Aerosol Sci. Technol.* **2012**, *46*, 719–749. [CrossRef]
30. Szybist, J.P.; Youngquist, A.D.; Barone, T.L.; Storey, J.M.; Moore, W.R.; Foster, M.; Confer, K. Ethanol Blends and Engine Operating Strategy Effects on Light-Duty Spark-Ignition Engine Particle Emissions. *Energy Fuels* **2011**, *25*, 4977–4985. [CrossRef]
31. Ntziachristos, L.; Amanatidis, S.; Samaras, Z.; Giechaskiel, B.; Bergmann, A. Use of a Catalytic Stripper as an Alternative to the Original PMP Measurement Protocol. *SAE Int. J. Fuels Lubr.* **2013**, *6*, 532–541. [CrossRef]
32. Gospodinova, S.; Miccoli, F. Commission Proposes New Euro 7 Standards to Reduce Pollutant Emissions from Vehicles and Improve Air Quality. European Commission. Available online: https://ec.europa.eu/commission/presscorner/detail/en/ip_22_6495 (accessed on 21 December 2022).
33. Samaras, Z.C.; Andersson, J.; Bergmann, A.; Hausberger, S.; Toumasatos, Z.; Keskinen, J.; Haisch, C.; Kontses, A.; Ntziachristos, L.D.; Landl, L.; et al. Measuring Automotive Exhaust Particles Down to 10 nm. *SAE Int. J. Adv. Curr. Pract. Mobil.* **2020**, *3*, 539–550. [CrossRef]
34. Samaras, Z.; Rieker, M.; Papaioannou, E.; Van Dorp, W.F.; Kousoulidou, M.; Ntziachristos, L.; Andersson, J.; Bergmann, A.; Hausberger, S.; Keskinen, J.; et al. Perspectives for regulating 10 nm particle number emissions based on novel measurement methodologies. *J. Aerosol Sci.* **2022**, *162*, 105957. [CrossRef]
35. Leach, F. *Particulate Emissions from Gasoline Direct Injection Engines*; Oxford University: Oxford, UK, 2014. Available online: https://ora.ox.ac.uk/objects/uuid:ea9c349e-5ade-4878-b758-c9a050c8f069 (accessed on 5 October 2022).
36. Pfau, S.A.; Haffner-Staton, E.; La Rocca, A. Measurement of Sub-23 nm Particulate Emissions from GDI Engines: A Comparison of Processing Methods. SAE Technical Paper 2021-01-0626. 2021. Available online: https://saemobilus.sae.org/papers/measurement-sub-23-nm-particulate-emissions-gdi-engines-a-comparison-processing-methods-2021-01-0626 (accessed on 21 December 2022). [CrossRef]
37. Pfau, S.A.; Haffner-Staton, E.; La Rocca, A.; Cairns, A. Investigating the Effect of Volatiles on Sub-23 nm Particle Number Measurements for a Downsized GDI Engine with a Catalytic Stripper and Digital Filtering. *Fuels* **2022**, *3*, 682–697. [CrossRef]
38. Leach, F.; Stone, R.; Richardson, D.; Lewis, A.; Akehurst, S.; Turner, J.; Remmert, S.; Campbell, S.; Cracknell, R.F. Particulate emissions from a highly boosted gasoline direct injection engine. *Int. J. Engine Res.* **2017**, *19*, 347–359. [CrossRef]
39. Leach, F.C.P.; Stone, R.; Richardson, D.; Turner, J.W.G.; Lewis, A.; Akehurst, S.; Sarah, R.; Steven, C.; Roger, C. The effect of oxygenate fuels on PN emissions from a highly boosted GDI engine. *Fuel* **2018**, *225*, 277–286. [CrossRef]
40. Leach, F.; Richardson, D.; Lewis, A.; Akehurst, S.; Turner, J. Sub-23 nm Particulate Emissions from a Highly Boosted GDI Engine. In Proceedings of the 14th International Conference on Engines & Vehicles, Napoli, Italy, 15–19 September 2019. [CrossRef]
41. Pfau, S.A.; La Rocca, A.; Haffner-Staton, E.; Fay, M.W.; Cairns, A. Linking operating conditions of a GDI engine to the nature and nanostructure of ultrafine soot particles. *Combust. Flame* **2022**, *245*, 112315. [CrossRef]
42. Schalla, R.L.; McDonald, G.E. Variation in Smoking Tendency Among Hydrocarbons of Low Molecular Weight. *Ind. Eng. Chem.* **1953**, *45*, 1497–1500. [CrossRef]
43. Lemaire, R.; Gwénolé, L.C.; Nakouri, M. Predicting the propensity to soot of hydrocarbons and oxygenated molecules by means of structural group contribution factors derived from the processing of unified sooting indexes. *Fuel* **2021**, *302*, 121104. [CrossRef]
44. Kittelson, D.B.; Watts, W.F.; Johnson, J.P. Diesel Aerosol Sampling Methodology—Crc E-43. 2002. Available online: https://citeseerx.ist.psu.edu/viewdoc/download?doi=10.1.1.378.3266&rep=rep1&type=pdf (accessed on 30 December 2022).
45. Wihersaari, H.; Pirjola, L.; Karjalainen, P.; Saukko, E.; Kuuluvainen, H.; Kulmala, K.; Keskinen, J.; Rönkkö, T. Particulate emissions of a modern diesel passenger car under laboratory and real-world transient driving conditions. *Environ. Pollut.* **2020**, *265*, 114948. [CrossRef]
46. Pirjola, L.; Karjalainen, P.; Heikkilä, J.; Saari, S.; Tzamkiozis, T.; Ntziachristos, L.; Kulmala, K.; Keskinen, J.; Rönkkö, T. Effects of Fresh Lubricant Oils on Particle Emissions Emitted by a Modern Gasoline Direct Injection Passenger Car. *Environ. Sci. Technol.* **2015**, *49*, 3644–3652. [CrossRef] [PubMed]
47. Okuyama, Y.; Shimokoji, D.; Sakurai, T.; Maruyama, M. Study of Low-Viscosity Engine Oil on Fuel Economy and Engine Reliability. In Proceedings of the SAE 2011 World Congress & Exhibition, Detroit, MI, USA, 12–14 April 2011. [CrossRef]
48. Sagawa, T.; Nakano, S.; Bito, Y.; Koike, Y.; Okuda, S.; Suzuki, R. Development of Low Viscosity API SN 0W-16 Fuel-Saving Engine Oil Considering Chain Wear Performance. *SAE Int. J. Fuels Lubr.* **2017**, *10*, 469–477. [CrossRef]

49. Lensch-Franzen, C.; Gohl, M.; Scholl, P.; Paoloni, F. Impact of Engine Lubricant Volatility on Oil and Particle Emissions. *MTZ Worldw.* **2019**, *80*, 44–53. [CrossRef]
50. Easter, J.; Bohac, S.; Hoard, J.; Boehman, A. Influence of ash-soot interactions on the reactivity of soot from a gasoline direct injection engine. *Aerosol Sci. Technol.* **2020**, *54*, 1373–1385. [CrossRef] [PubMed]
51. Zinola, S.; Rouleau, L.; Dunand, X.; Baltzopoulou, P.; Chasapidis, L.; Deloglou, D.; Melas, A.D.; Konstandopoulos, A.G.; Rüggeberg, T.; Fierz, M.; et al. Measurement of Sub-23 nm particles emitted by gasoline direct injection engine with new advanced instrumentation. In Proceedings of the 2019 JSAE/SAE Powertrains, Fuels and Lubricants, Winchester, UK, 4–6 December 2019. [CrossRef]
52. Lähde, T.; Giechaskiel, B.; Martini, G.; Howard, K.; Jones, J.; Ubhi, S. Effect of lubricating oil characteristics on solid particle number and $CO_2$ emissions of a Euro 6 light-duty compressed natural gas fuelled vehicle. *Fuel* **2022**, *324*, 124763. [CrossRef]
53. Guido, C.; Napolitano, P.; Di Domenico, D.; Di Maio, D.; Beatrice, C.; Griffaton, B.; Obrecht, N. Exploiting Lubricant Formulation to Reduce Particle Emissions from Gas Powered Engines. *Energies* **2024**, *17*, 3781. [CrossRef]
54. Premnath, V.; Khalek, I.; Morgan, P.; Michlberger, A.; Sutton, M.; Vincent, P. Effect of Lubricant Oil on Particle Emissions from a Gasoline Direct Injection Light-Duty Vehicle. SAE Technical Paper 2018-01-1708. 2018. Available online: https://saemobilus.sae.org/papers/effect-lubricant-oil-particle-emissions-a-gasoline-direct-injection-light-duty-vehicle-2018-01-1708 (accessed on 30 December 2022).
55. *EN 228:2008*; Automotive Fuels—Unleaded Petrol—Requirements and Test Methods. European Committee for Standardization (CEN): Brussels, Belgium, 2008.
56. Gaddam, C.K. *Physical and Chemical Characterization of Gasoline Particulates and Differences Relative to Diesel Soot*; Pennsylvania State University: University Park, PA, USA, 2012. Available online: https://etda.libraries.psu.edu/files/final_submissions/7062 (accessed on 8 March 2023).
57. *ASTM D2270-24*; Standard Practice for Calculating Viscosity Index from Kinematic Viscosity at 40 °C and 100 °C. ASTM International: West Conshohocken, PA, USA, 2024.
58. *ASTM D4683-20*; Standard Test Method for Measuring Viscosity of New and Used Engine Oils at High Shear Rate and High Temperature by Tapered Bearing Simulator Viscometer at 150 °C. ASTM International: West Conshohocken, PA, USA, 2020.
59. *ASTM D5293-20*; Standard Test Method for Apparent Viscosity of Engine Oils and Base Stocks Between −10 °C and −35 °C Using Cold-Cranking Simulator. ASTM International: West Conshohocken, PA, USA, 2020.
60. *ASTM D5800-21*; Standard Test Method for Evaporation Loss of Lubricating Oils by the Noack Method. ASTM International: West Conshohocken, PA, USA, 2021.
61. Kumar, P.; Fennell, P.; Symonds, J.; Britter, R. Treatment of losses of ultrafine aerosol particles in long sampling tubes during ambient measurements. *Atmos. Environ.* **2008**, *42*, 8819–8826. [CrossRef]
62. Miller, A.L.; Stipe, C.B.; Habjan, M.C.; Ahlstrand, G.G. Role of Lubrication Oil in Particulate Emissions from a Hydrogen-Powered Internal Combustion Engine. *Environ. Sci. Technol.* **2007**, *41*, 6828–6835. [CrossRef] [PubMed]
63. Nowak, N.; Sinn, T.; Scheiber, K.; Straube, C.; Pfeil, J.; Meyer, J.; Koch, T.; Kasper, G.; Dittler, A. On aerosol formation by condensation of oil vapor in the crankcase of combustion engines. *Aerosol Sci. Technol.* **2022**, *56*, 101–116. [CrossRef]